

Extending a previous analysis on a possible modulation effect in WIMP direct search

A. Bottino^{a*}, F. Donato^a, N. Fornengo^a, S. Scopel^{b†}

^a *Dipartimento di Fisica Teorica, Università di Torino and
INFN, Sezione di Torino, Via P. Giuria 1, 10125 Torino, Italy*

^b *Instituto de Física Nuclear y Altas Energías,
Facultad del Ciencias, Universidad de Zaragoza,
Plaza de San Francisco s/n, 50009 Zaragoza, Spain*

(October 9, 1997)

Abstract

In this note we present an extension of our previous analysis of some preliminary experimental results of the DAMA/NaI Collaboration which might be indicative of a yearly modulation effect. Here we present a direct way for obtaining from the experimental data the relevant cosmological implications for relic neutralinos. We find that some of the configurations singled out by the DAMA/NaI results would have cosmological properties compatible with a neutralino as a dominant component of cold dark matter (on the average in the Universe and in our galactic halo).

Typeset using REVTeX

*E-mail: bottino@to.infn.it, donato@to.infn.it, fornengo@to.infn.it, scopel@posta.unizar.es

†INFN Post-doctoral Fellow

Some recent results of the DAMA/NaI Collaboration on direct WIMP detection [1] seem to indicate that a yearly modulation effect might be present. As stressed in Ref. [1], a much larger statistics is necessary, before any claim of a real effect can be made; and, actually, a further collection of data is under way at the large-mass, low-background NaI(Tl) detector at the Gran Sasso Laboratory [1]. Meanwhile, the preliminary results are so intriguing to prompt an analysis of their possible implications for particle physics and cosmological properties.

In Ref. [2], we have analyzed some possible consequences for neutralino properties implied by the results of Ref. [1], under the hypothesis that these are indicative of a yearly modulation effect due to relic neutralinos. We have shown that a number of neutralino configurations, compatible with all current experimental constraints, might produce a modulation effect at the level of the one possibly detected by the DAMA/NaI Group. Some appealing features of these configurations (or at least of a subset of these) are: i) sizeable cosmological density Ω , ii) detectability of indirect signals at neutrino telescopes, iii) detectability of some related properties at accelerators.

In our previous paper [2] the comparison of theoretical evaluations with experimental data was performed in terms of a plot in the plane $\xi\sigma_{\text{scalar}}^{(\text{nucleon})}$ vs. m_χ , where m_χ is the neutralino mass, $\sigma_{\text{scalar}}^{(\text{nucleon})}$ is the scalar elastic cross section off nucleon and $\xi = \rho_\chi/\rho_l$ is the fractional amount of local neutralino dark matter density ρ_χ with respect to the total local dark matter density ρ_l . The results are reported in Fig. 1 (which is taken from Ref. [2]). The closed contour line denotes the region (R_m) singled out at 90% C.L. by the data of Ref. [1]. The open curve denotes the 90% C.L. upper bound of $\xi\sigma_{\text{scalar}}^{(\text{nucleon})}$, as obtained from the total counting rates of Ref. [3]. In extracting both the open and the closed contour lines from the experimental data, the values of some astrophysical parameters relevant for the event rates at the detector have to be chosen. These parameters are: the root mean square velocity v_{rms} of the neutralino Maxwellian velocity distribution in the halo, the neutralino escape velocity v_{esc} in the halo, the velocity v_\odot of the Sun around the galactic centre. The values adopted in Fig. 1 refer to the median values of these parameters in their experimentally allowed ranges [4], namely: $v_{\text{rms}} = 270 \text{ Km s}^{-1}$, $v_{\text{esc}} = 650 \text{ Km s}^{-1}$, $v_\odot = 232 \text{ Km s}^{-1}$. We remark that the values of $\xi\sigma_{\text{scalar}}^{(\text{nucleon})}$, extracted from experimental data, are not very sensitive to the specific values adopted for the various velocities within their physical ranges. The values of $\xi\sigma_{\text{scalar}}^{(\text{nucleon})}$ plotted in Fig. 1 are normalized to the value $\rho_l = 0.5 \text{ GeV cm}^{-3}$.

Together with the experimental results, Fig. 1 shows our evaluations of the quantity $\xi\sigma_{\text{scalar}}^{(\text{nucleon})}$ inside the Minimal Supersymmetric Standard Model. For a brief discussion of the model we are employing, the reader is addressed to Ref. [2]. Here we only recall that the supersymmetric parameter space, considered here and in Ref. [2], consists of six independent parameters: $M_2, \mu, \tan\beta, m_A, m_0, A$. We vary these parameters in the following ranges: $10 \text{ GeV} \leq M_2 \leq 500 \text{ GeV}$ (21 steps over a linear grid); $10 \text{ GeV} \leq |\mu| \leq 500 \text{ GeV}$ (21 steps, linear grid); $65 \text{ GeV} \leq m_A \leq 500 \text{ GeV}$ (15 steps, logarithmic grid); $100 \text{ GeV} \leq m_0 \leq 500 \text{ GeV}$ (5 steps, linear grid); $-3 \leq A \leq +3$ (5 steps, linear grid); $1.01 \leq \tan\beta \leq 50$ (15 steps, logarithmic grid).

The supersymmetric parameter space is constrained by the experimental limits obtained from accelerators on supersymmetric and Higgs searches and from the $b \rightarrow s + \gamma$ radiative decay. For a complete set of references, see Ref. [2]. In addition to the experimental limits,

the parameter space is further constrained by the requirement that the neutralino is the lightest supersymmetric particle, since the neutralino is the dark matter candidate under investigation in the present analysis. Finally, the regions of the parameter space where the neutralino relic abundance exceeds the cosmological bound, i.e. $\Omega_\chi h^2 > 1$, are also excluded.

Our analysis in Ref. [2] was performed employing, for the evaluation of ξ , the usual rescaling recipe [5] which compares the amount of neutralino relic density $\Omega_\chi h^2$ to the minimal value for the total amount of dark matter in the Universe compatible with observational data and with large-scale structure calculations. The recipe works as follows: when $\Omega_\chi h^2$ is larger than $(\Omega h^2)_{\min}$ we simply put $\xi = 1$; when $\Omega_\chi h^2$ turns out to be less than $(\Omega h^2)_{\min}$, and then the neutralino may only provide a fractional contribution $\Omega_\chi h^2 / (\Omega h^2)_{\min}$ to Ωh^2 , we take $\xi = \Omega_\chi h^2 / (\Omega h^2)_{\min}$.

Besides the empirical character of the rescaling procedure, it has to be noted that, as was stressed in Ref. [2], the value of $(\Omega h^2)_{\min}$ is rather arbitrary, possibly in the range $0.03 \lesssim (\Omega h^2)_{\min} \lesssim 0.3$. To be definite, in Ref. [2] we reported our results for the representative value $(\Omega h^2)_{\min} = 0.03$, and this is the value used in the scatter plot of Fig. 1.

In this note we present an extension of our previous investigation, which is meant to obtain from the experimental data the relevant cosmological implications for relic neutralinos, in the most direct way without any use of rescaling for the neutralino local density.

The procedure we adopt is the following: 1) We evaluate $\sigma_{\text{scalar}}^{(\text{nucleon})}$ and $\Omega_\chi h^2$ by varying the supersymmetric parameters over the previously defined grid. 2) For any value of $[\rho_\chi \sigma_{\text{scalar}}^{(\text{nucleon})}]_{\text{expt}} = \rho_l [\xi \sigma_{\text{scalar}}^{(\text{nucleon})}]_{\text{expt}}$ compatible with the experimental region R_m we calculate ρ_χ as given by $\rho_\chi = [\rho_\chi \sigma_{\text{scalar}}^{(\text{nucleon})}]_{\text{expt}} / \sigma_{\text{scalar}}^{(\text{nucleon})}$ and restrict the values of m_χ to stay inside the region R_m . 3) The results are displayed in a scatter plot in the plane ρ_χ vs. $\Omega_\chi h^2$.

Examples of our results are given in Figs. 2–4 for a few experimentally allowed values of $\xi \sigma_{\text{scalar}}^{(\text{nucleon})}$, taken from Fig. 1 (remember that the normalization value $\rho_l = 0.5 \text{ GeV cm}^{-3}$ is used in this figure). Figs. 2,3,4 refer to $[\xi \sigma_{\text{scalar}}^{(\text{nucleon})}]_{\text{expt}} = 6 \cdot 10^{-9} \text{ nbarn}$, $2 \cdot 10^{-9} \text{ nbarn}$ and $1 \cdot 10^{-9} \text{ nbarn}$, respectively. The two horizontal lines denote the physical range $0.1 \text{ GeV cm}^{-3} < \rho_l < 0.7 \text{ GeV cm}^{-3}$ for the local density of non-baryonic dark matter. This (rather generous) range has been established by taking into account possible effects on ρ_l due to a flattened dark halo [6] and a recent derivation [7] of the contribution of baryons to the local dark matter from microlensing data. The solid vertical lines denote the physical band for Ωh^2 : $0.03 \lesssim \Omega h^2 \lesssim 1$, and the two dashed lines give the favored band for the cold dark matter contribution to Ω : $0.1 < (\Omega h^2)_{\text{CDM}} < 0.3$ [8]. The two tilted dot-dashed lines denote the band where linear rescaling procedure for the local density is usually applied. The upper dot-dashed line refers to a rescaling with $(\Omega h^2)_{\min} = 0.03$, the lower one to the value $(\Omega h^2)_{\min} = 0.3$. With the aid of this kind of plot we can classify the supersymmetric configurations belonging to region R_m into various categories. Configurations whose representative points fall above the maximum value $\rho_\chi = 0.7 \text{ GeV cm}^{-3}$ have to be excluded (we remind that those providing an $\Omega_\chi h^2 > 1$ are already disregarded from the very beginning). Among the allowed configurations, those falling in the region inside both the horizontal and solid vertical lines (this region is called *A* hereafter) are very appealing, since they would represent situations where the neutralino could have the role of a dominant cold dark matter component; even more so, if the representative points fall in the subregion (*B*) inside the vertical band delimited by dashed lines. Configurations which fall inside the band delimited

by the tilted dot-dashed lines denotes situations where the neutralino can only provide a fraction of the cold dark matter both at the level of local density and at the level of the average Ω . Configurations above the upper dot-dashed line and below the upper solid horizontal line would imply an unlikely special clustering of neutralinos in our halo as compared to their average distribution in the Universe.

It is worth noticing a few important properties of the scatter plots shown in Figs. 2–4:

- 1) The scatter plots display a correlation between ρ_χ and $\Omega_\chi h^2$. This feature is expected on the basis of the following properties: i) $\Omega_\chi h^2$ is roughly inversely proportional to the neutralino pair annihilation cross section, ii) at fixed $[\xi\sigma_{\text{scalar}}^{(\text{nucleon})}]_{\text{expt}}$, ρ_χ is inversely proportional to $\sigma_{\text{scalar}}^{(\text{nucleon})}$, iii) the annihilation cross section and $\sigma_{\text{scalar}}^{(\text{nucleon})}$ are usually correlated functions (i.e., they are both increasing or decreasing functions of the supersymmetric parameters).
- 2) The regions *A* and *B* become more populated in configurations as the experimental value $[\xi\sigma_{\text{scalar}}^{(\text{nucleon})}]_{\text{expt}}$ decreases (i.e., if one proceeds from the case shown in Fig. 2 to the one in Fig. 4). This feature follows from the fact that $\sigma_{\text{scalar}}^{(\text{nucleon})}$ is bounded from above by accelerator limits (mainly because of lower bounds on Higgs masses); this implies for ρ_χ a lower bound, which however is less stringent at lower values of $[\xi\sigma_{\text{scalar}}^{(\text{nucleon})}]_{\text{expt}}$.
- 3) It is remarkable that, as a consequence of point 2), some neutralino configurations populate the most interesting region, i.e. region *B*. This occurs for $[\xi\sigma_{\text{scalar}}^{(\text{nucleon})}]_{\text{expt}} \lesssim 6 \cdot 10^{-9}$ nbarn.

In what follows we concentrate on configurations falling in region *A* or in the subregion *B*. For definiteness, we choose the representative value $[\xi\sigma_{\text{scalar}}^{(\text{nucleon})}]_{\text{expt}} = 2 \cdot 10^{-9}$ nbarn. First, we check whether some of these neutralino compositions are excluded by indirect detection of WIMPs, by measurements of up-going muon fluxes due to the neutrino outburst produced by neutralino pair annihilation in the Earth or in the Sun. In Fig. 5 we show how our calculated fluxes from the Earth Φ_μ^{Earth} compare with the current experimental upper bounds [9,10]. We notice that some configurations are actually excluded by the present limits on Φ_μ^{Earth} . From our calculations, it turns out that the present upper bounds on the up-going muon fluxes from the Sun constrain the analyzed configurations only marginally.

Finally, we provide in Figs. 6,7 some information about important parameters referring to the configurations of region *A* and of subregion *B*. These figures also show what may be the exploration potential for these configurations at LEP2 and Tevatron.

In conclusion, we remark that our present analysis shows, in a way independent of the rescaling procedure on local DM density, that some of the configurations singled out by the DAMA/NaI results would have cosmological properties compatible with a neutralino as a dominant component of cold dark matter (on the average in the Universe and in our galactic halo).

REFERENCES

- [1] R. Bernabei et al., ROM2F/97/33, September 1997;
P. Belli, talk at TAUP97, Laboratori Nazionali del Gran Sasso, September 1997;
P. Belli, talk at COSMO97, Ambleside, England, September 1997.
- [2] A. Bottino, F. Donato, N. Fornengo, S. Scopel, DFTT 49/97, September 1997, [hep-ph/9709292](#);
F. Donato, talk at TAUP97, Laboratori Nazionali del Gran Sasso, September 1997;
S. Scopel, talk at COSMO97, Ambleside, England, September 1997.
- [3] R. Bernabei et al., Phys. Lett. B 389 (1996) 757.
- [4] A. Bottino, F. Donato, G. Mignola, S. Scopel, P. Belli and A. Incicchitti, Phys. Lett. B 402 (1997) 113.
- [5] T.K. Gaisser, G. Steigman and S. Tilav, Phys. Rev. D34 (1986) 1023
- [6] E. Gates, G. Gyuk and M.S. Turner, Phys. Rev. Lett. 74 (1995) 3724; Astrophys. J. Lett. 449 (1995) L123; Phys. Rev. D53 (1996) 4138.
- [7] E. Gates, G. Gyuk and M.S. Turner, talk presented at 18th Texas Symposium on Relativistic Astrophysics, Chicago, IL, 15–20 Dec 1996, [astro-ph/9704253](#).
- [8] V. Berezhinsky, A. Bottino, J. Ellis, N. Fornengo, G. Mignola and S. Scopel, Astropart. Phys. 5 (1996) 333.
- [9] O. Suvorova, Baksan Collab., talk at the 4th Int. Neutrino Conference, Heidelberg, April 1997
- [10] F. Ronga, Macro Collab., talk at the 25th Int. Cosmic Ray Conference (ICRC 97), Durban, South Africa, July 1997;
T. Montaruli, Macro Collab., talk at TAUP97, Laboratori Nazionali del Gran Sasso, September 1997.
- [11] ALEPH Collab., CERN-PPE/97-041, April 1997;
ALEPH Collab., CERN-PPE/97-056, May 1997;
ALEPH Collab., CERN-PPE/97-071, June 1997;
A. De Min, DELPHI Collab., talk at the 3rd Warsaw Workshop ‘Physics from the Planck scale to the electroweak scale’, Warsaw, April 1997;
DELPHI Collab., CERN-PPE/97-085, July 1997;
F. Di Lodovico, L3 Collab., talk at the 3rd Warsaw Workshop ‘Physics from the Planck scale to the electroweak scale’, Warsaw, April 1997;
OPAL Collab., CERN-PPE/97-046, April 1997;
OPAL Collab., CERN-PPE/97-083, July 1997.
- [12] Physics at LEP2, editors G. Altarelli, T. Sjöstrand and F. Zwirner, CERN 96-01, February 1996.
- [13] Report of the TeV-2000 Study Group, editors D. Amidei and R. Brock, FERMILAB-PUB-96/082, April 1996.

FIGURE CAPTIONS

Figure 1 – The scalar neutralino–nucleon cross section $\sigma_{\text{scalar}}^{(\text{nucleon})}$, multiplied by the factor ξ , is plotted versus the neutralino mass m_χ . The closed contour delimits the region singled out at 90% C.L. by the data of Ref. [1]. The open curve denotes the 90% C.L. upper bound obtained from the total counting rates of Ref. [3]. The scatter plot represents the theoretical prediction for $\xi\sigma_{\text{scalar}}^{(\text{nucleon})}$, calculated within the MSSM scheme. Only configurations with $\mu > 0$ are displayed. The cosmological and astrophysical parameters are set to the following values: $v_{\text{rms}} = 270 \text{ Km s}^{-1}$, $v_{\text{esc}} = 650 \text{ Km s}^{-1}$, $v_\odot = 232 \text{ Km s}^{-1}$, $\rho_l = 0.5 \text{ GeV cm}^{-3}$ and $(\Omega h^2)_{\text{min}} = 0.03$.

Figure 2 – The neutralino local density ρ_χ , calculated for $[\xi\sigma_{\text{scalar}}^{(\text{nucleon})}]_{\text{expt}} = 6 \cdot 10^{-9}$ nbarn, is plotted versus the neutralino relic abundance $\Omega_\chi h^2$. For the value of $[\xi\sigma_{\text{scalar}}^{(\text{nucleon})}]_{\text{expt}}$ employed here, the neutralino mass is restricted to the range $30 \text{ GeV} \lesssim m_\chi \lesssim 155 \text{ GeV}$, as obtained from the closed contour in Fig. 1. The two horizontal lines denote the physical range for the local density of non–baryonic dark matter. The two solid vertical lines denote the physical band for Ωh^2 , and the two dashed lines give the preferred band for the cold dark matter contribution to Ω . The two tilted dot–dashed lines denote the band where linear rescaling procedure for the local density is usually applied. The region inside both the two horizontal lines and the two vertical solid (dashed) lines is defined as region *A* (region *B*).

Figure 3 – The neutralino local density ρ_χ , calculated for $[\xi\sigma_{\text{scalar}}^{(\text{nucleon})}]_{\text{expt}} = 2 \cdot 10^{-9}$ nbarn, is plotted versus the neutralino relic abundance $\Omega_\chi h^2$. The neutralino mass is restricted to the range $30 \text{ GeV} \lesssim m_\chi \lesssim 115 \text{ GeV}$, as obtained from the closed contour in Fig. 1. The solid, dashed and dot–dashed lines, as well as region *A* and region *B*, are defined as in Fig. 2.

Figure 4 – The neutralino local density ρ_χ , calculated for $[\xi\sigma_{\text{scalar}}^{(\text{nucleon})}]_{\text{expt}} = 1 \cdot 10^{-9}$ nbarn, is plotted versus the neutralino relic abundance $\Omega_\chi h^2$. The neutralino mass is restricted to the range $40 \text{ GeV} \lesssim m_\chi \lesssim 85 \text{ GeV}$, as obtained from the closed contour in Fig. 1. The solid, dashed and dot–dashed lines, as well as region *A* and region *B*, are defined as in Fig. 2.

Figure 5 – Flux of up–going muons Φ_μ^{Earth} as a function of the neutralino mass m_χ , calculated for the neutralino configurations belonging to region *A* (dots) and to region *B* (crosses) of Fig. 3 (therefore referring to $[\xi\sigma_{\text{scalar}}^{(\text{nucleon})}]_{\text{expt}} = 2 \cdot 10^{-9}$ nbarn and $40 \text{ GeV} \lesssim m_\chi \lesssim 115 \text{ GeV}$). The solid and dashed lines represent the experimental 90% C.L. upper bounds of Ref. [9] and Ref. [10], respectively.

Figure 6 – The configurations compatible with region *A* (dots) and region *B* (crosses) of Fig. 3 are plotted in the m_χ – $\tan\beta$ plane. Configurations which provide a flux of up–going muons exceeding the experimental upper limits of Ref. [9,10] are dropped. The dark region on the left side is excluded by current LEP data [11]. The region on the left of the vertical solid line will be accessible to LEP at $\sqrt{s} = 192 \text{ GeV}$ [12]. The region on the left of the vertical dashed line will be explorable at TeV33 [13].

Figure 7 – The configurations compatible with region A (dots) and region B (crosses) of Fig. 3 are plotted in the m_h - $\tan \beta$ plane. Configurations which provide a flux of up-going muons exceeding the experimental upper limits of Ref. [9,10] are dropped. The dark regions are excluded by current LEP searches [11] or by theoretical arguments. The region on the left of the solid line will be accessible to LEP at $\sqrt{s} = 192$ GeV, with a luminosity of 150 pb^{-1} per experiment [12].

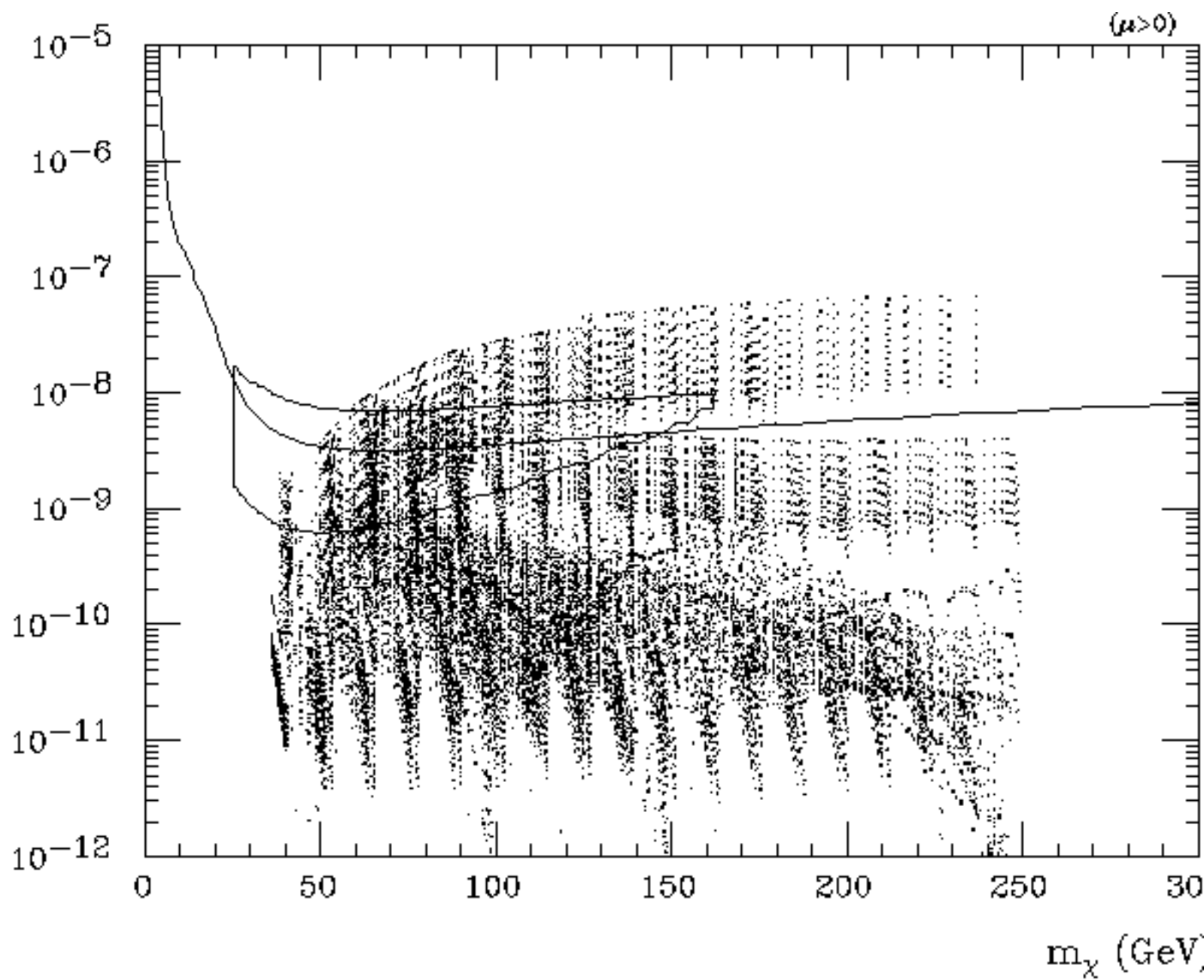


Figure 1

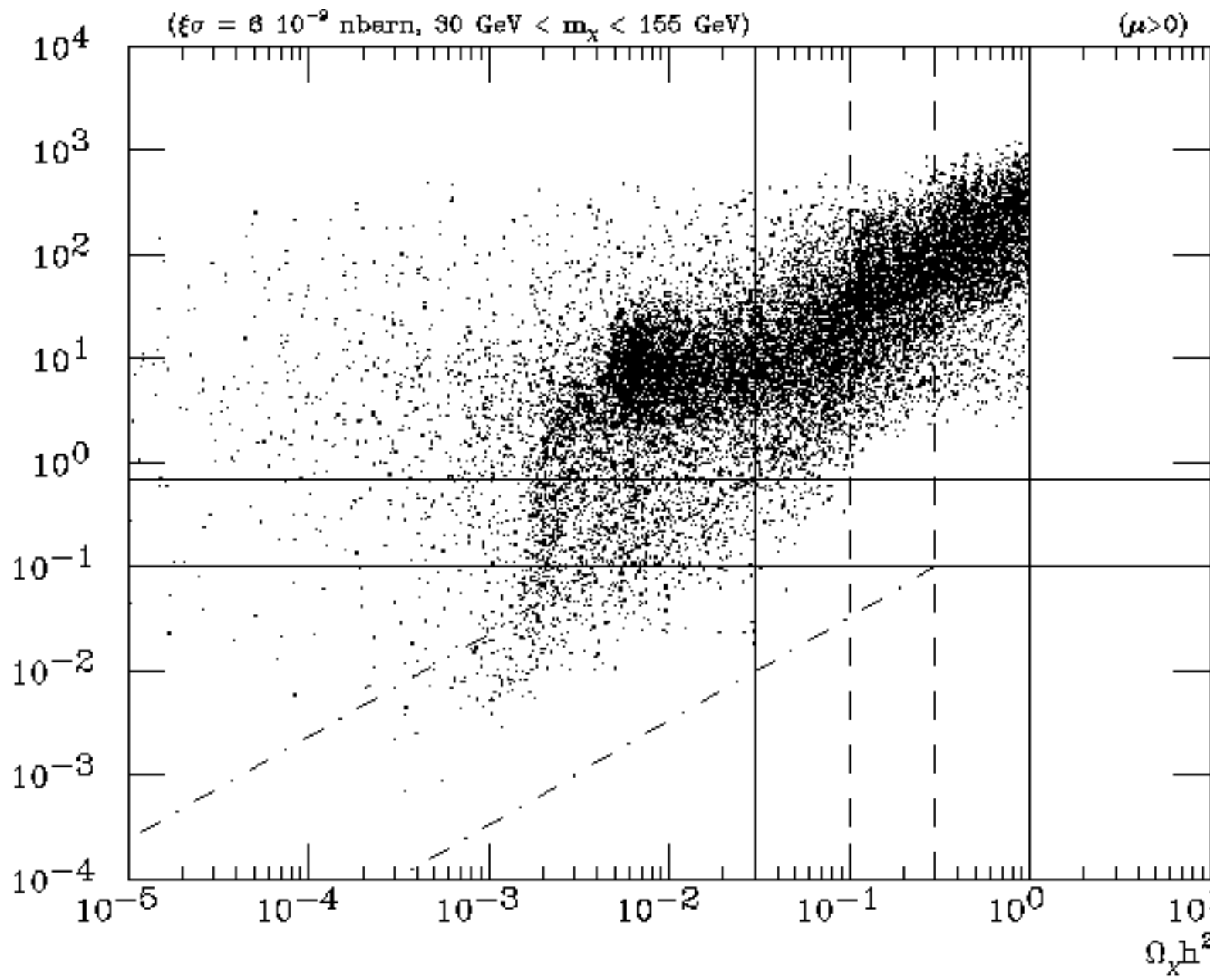


Figure 2

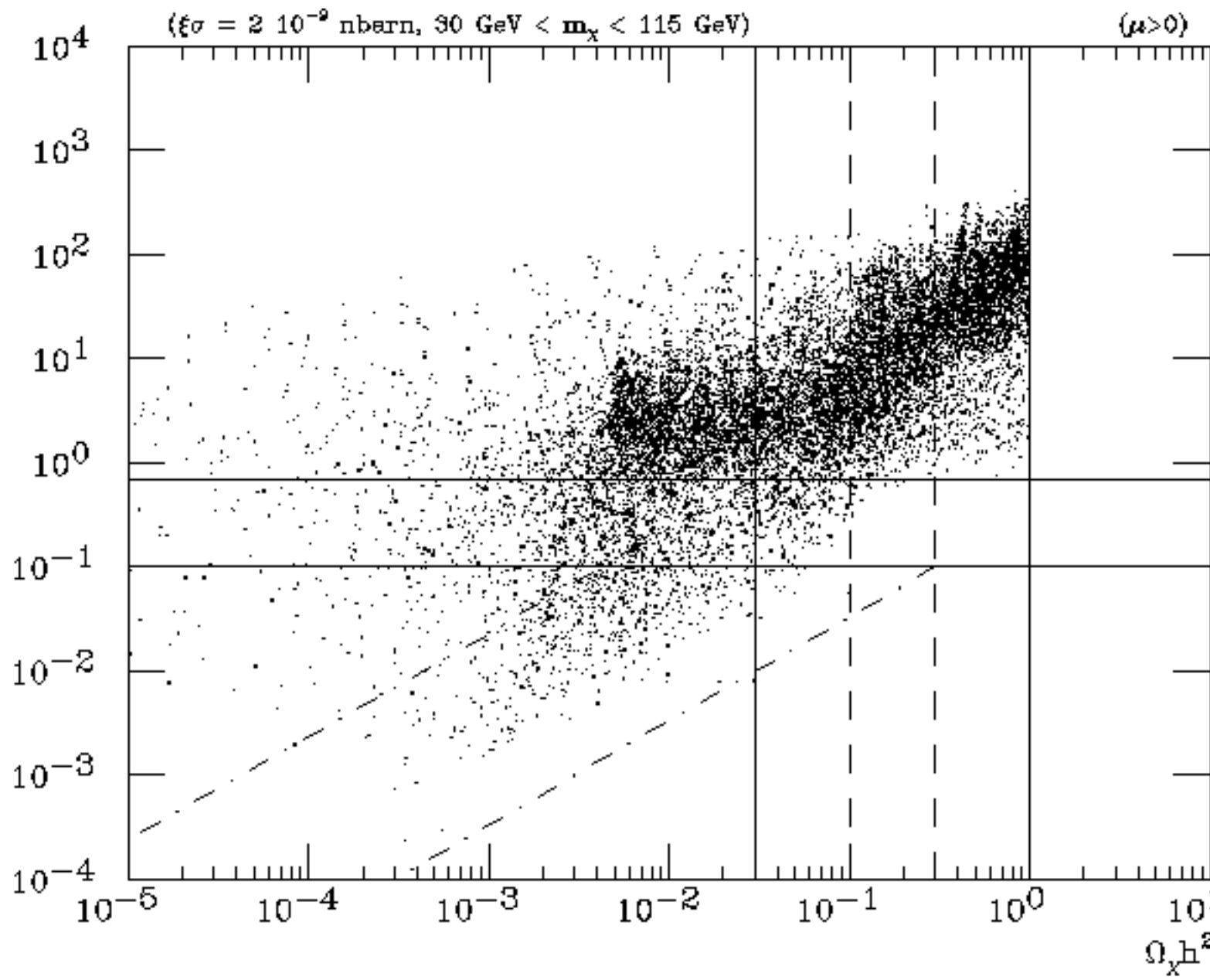


Figure 3

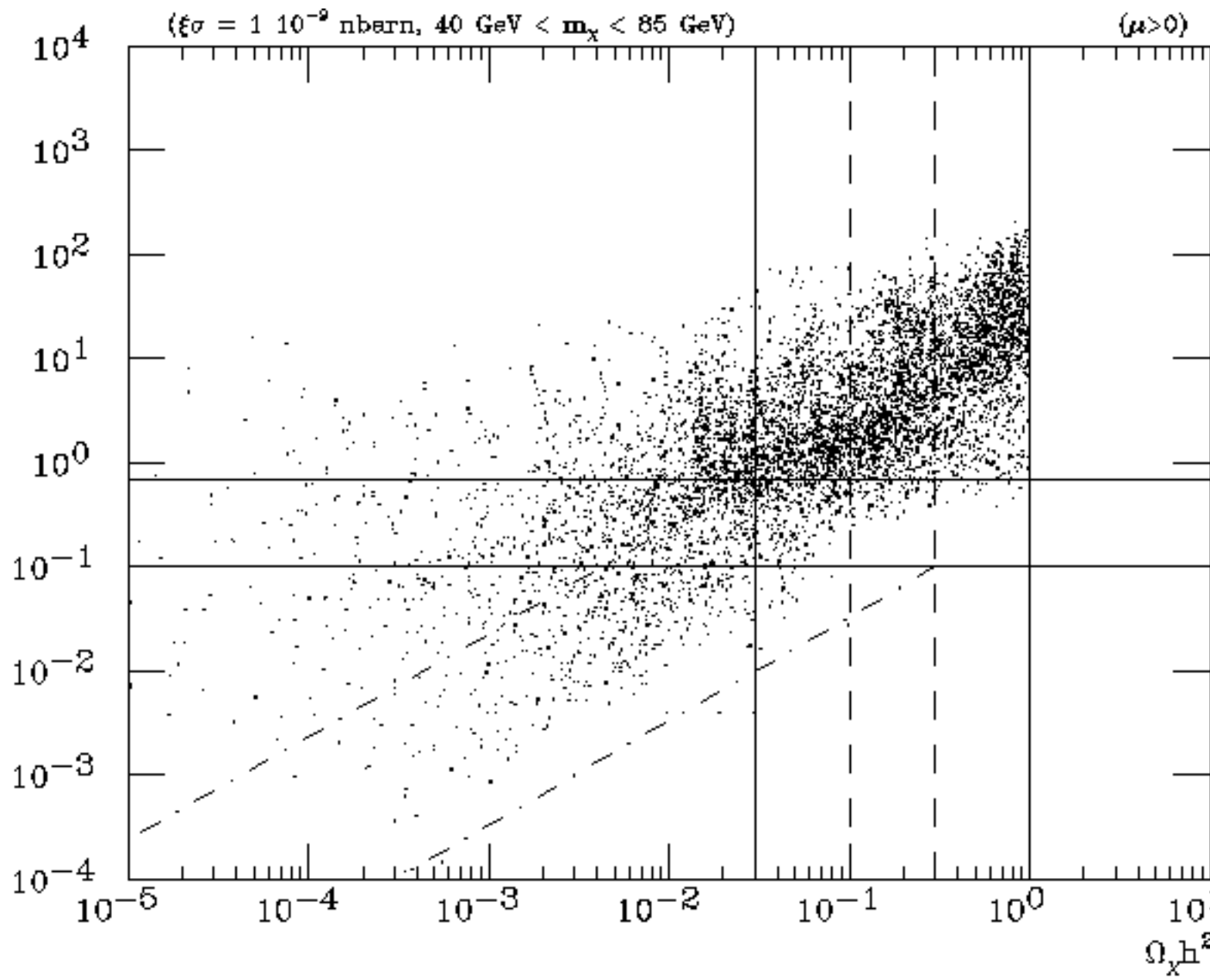


Figure 4

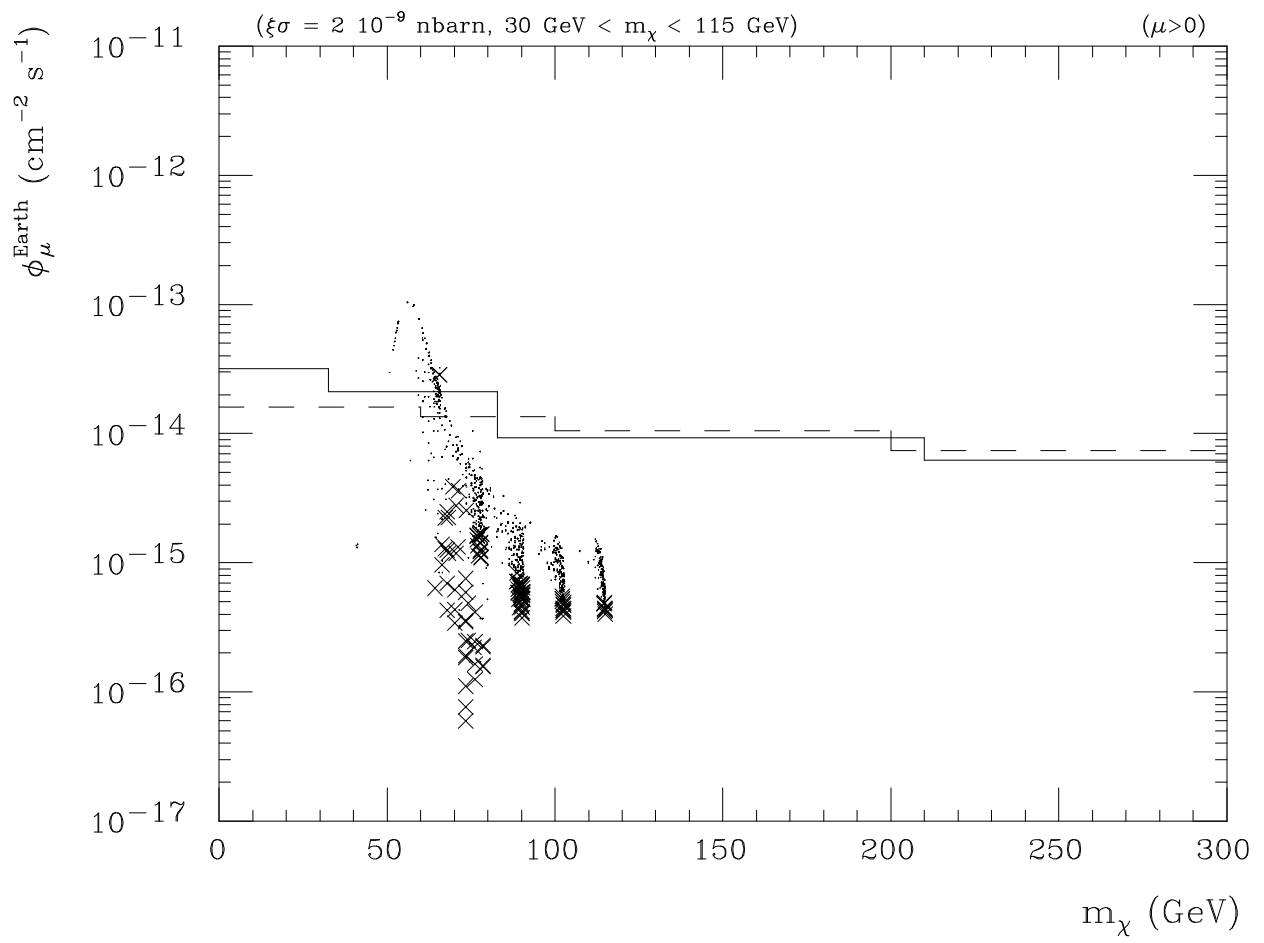


Figure 5

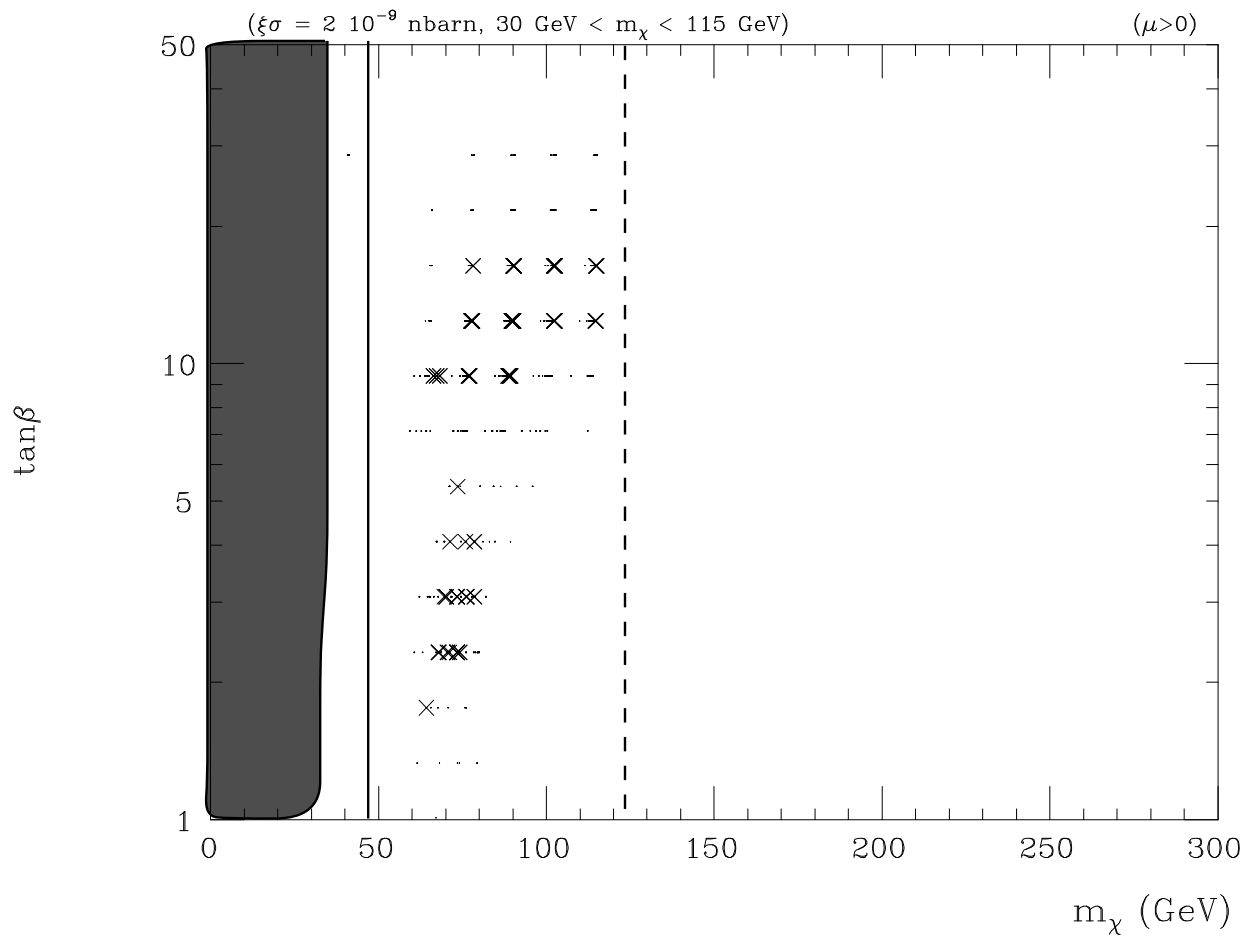


Figure 6

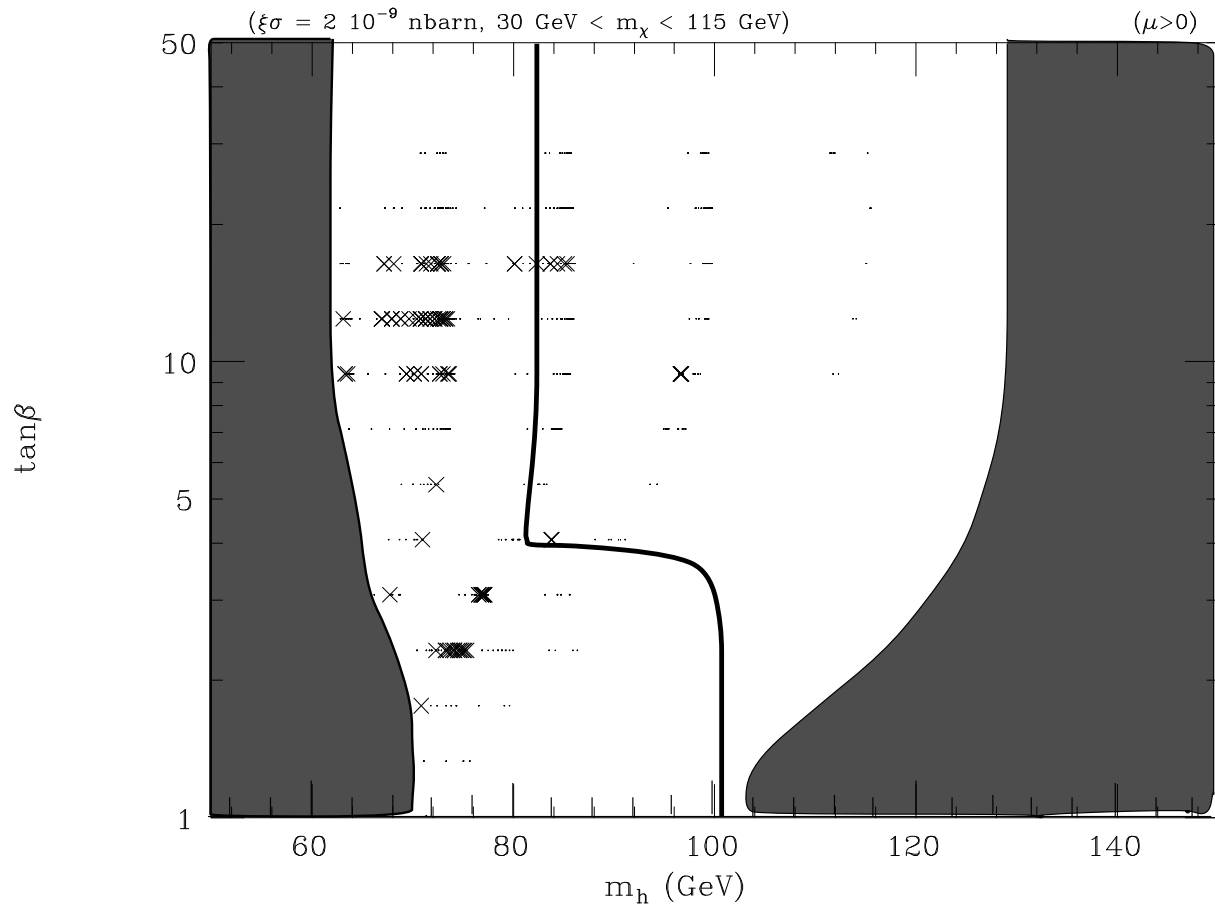


Figure 7